# Tensile-stress-induced growth of ellipsoidal ω-precipitates in a Ti–20wt%Mo alloy

# Tensile-stress-induced growth of ellipsoidal ω-precipitates in a Ti–20wt%Mo alloy

**Ryoichi Monzen·Ryutaro Kawai·Toru Oyama·Chihiro Watanabe**

R. Monzen[a]*

[a] Division of Mechanical Science and Engineering, Graduate School of Natural Science and Technology, Kanazawa University, Kakuma-machi, Kanazawa 920-1192, Japan

TEL: +81-76-234-4678

* Corresponding author, E-mail: monzen@se.kanazawa-u.ac.jp

R. Kawai[a]

[a] Division of Mechanical Science and Engineering, Graduate School of Natural Science and Technology, Kanazawa University, Kakuma-machi, Kanazawa 920-1192, Japan

E-mail: ryutaro262@gmail.com

TEL: +81-76-234-4681

T. Oyama[a]

[a] Division of Mechanical Science and Engineering, Graduate School of Natural Science and Technology, Kanazawa University, Kakuma-machi, Kanazawa 920-1192, Japan

E-mail: mineraru@stu.kanazawa-u.ac.jp

TEL: +81-76-234-4681

C. Watanabe[a]

[a] Division of Mechanical Science and Engineering, Graduate School of Natural Science and Technology, Kanazawa University, Kakuma-machi, Kanazawa 920-1192, Japan

E-mail: chihiro@se.kanazawa-u.ac.jp

TEL: +81-76-234-4679

**Abstract** The effects of applied tensile stress on the growth of ellipsoidal ω phase precipitates have been investigated for a Ti–20wt%Mo alloy aged at 300 °C. The application of tensile stress accelerates the growth of ω-precipitates when the misfit strain $\varepsilon_M$ of the precipitates along the loading direction is greater than 0; however, it does not significantly affect the growth of precipitates in cases where $\varepsilon_M < 0$. Whereas the growth of precipitates under no stress or in the case where $\varepsilon_M < 0$ under tensile stress is governed by the diffusion of Mo from the ω/β interface toward the β-Ti matrix, precipitate growth is instead interface-controlled in the case where $\varepsilon_M > 0$ under a tensile stress of 400 – 550 MPa. The growth velocity of precipitates in the case where $\varepsilon_M > 0$ is proportional to the tensile stress. This result, together with the misfit strain dependence of the growth of precipitates, is discussed on the basis of the interaction energy between the stress acting on a ω-precipitate and its misfit strain. The activation energies for the diffusion-controlled and interface-controlled growth are estimated to be approximately 190 and 130 kJ/mol, respectively. The value of 190 kJ/mol is consistent with the activation energy for volume diffusion of Mo in β-Ti.

**Key words:** Ti-Mo alloy; ω-precipitates; growth; applied tensile stress; misfit; interaction energy

## Introduction

The application of elastic stress during the aging process of Al–Cu [1-4], Al–Zn–Mg–Cu [5], and Cu–Be [6, 7] alloys is well known to significantly affect the alloys' resulting microstructures, particularly the distribution of precipitates. Stress on the precipitate distribution is believed to affect the nucleation process of precipitates [2, 3, 6, 7]. However, few experimental investigations of the effect of applied stress on the growth of precipitates have been reported.

Monzen et al. [7] have examined the effects of external stress on the nucleation and growth of disk-shaped γ″-phase precipitates in a Cu–1.2Be–0.1Co (All compositions in this text are expressed by weight per cent, wt%) alloy aged at 320 °C. The metastable γ″-phase comprises alternating Be and Cu matrix layers parallel to the $\{100\}_\alpha$ planes. A compressive stress applied in the [001] direction during aging preferentially accelerates the nucleation and growth of the γ″-variant normal to the [001] axis among the three crystallographically-equivalent variants. However, a tensile stress does not significantly affect the nucleation and growth of γ″-precipitates. The acceleration of the nucleation and growth of the specific γ″-variants can be understood through the interaction energy between the stress acting on the γ″-variants and their misfit strains.

Very recently, Monzen et al. [8] examined the formation of ellipsoidal ω-phase precipitates in a Ti-20Mo alloy aged at 300 °C under an external stress. The ω-precipitates have an ellipsoidal shape elongated along $<111>_\beta$ of the β-Ti matrix, with an aspect ratio of about 2 [9]. The application of tensile stress during aging promotes the nucleation of ω-precipitates; however, compressive stress does not essentially induce the same effect. Estimates of the average misfit strains along the loading direction and the transverse direction, where such estimates are based on the misfit strains of ω-precipitates and are calculated, from

measurements of the length change and the lattice parameter reveal the preferential formation of specific ω-variants among four crystallographically-equivalent variants, which depends on the sense of the applied stress. This is supported by the result related to the dependence of the number density of an ω-variant on its misfit strain along the loading direction. The dependences of the nucleation of ω precipitates and the formation of specific ω-variants on the sense of the applied stress are explained by the interaction energy due to the presence of misfit strains between the applied stress and the ω precipitate.

In this work, as an extension of our previous study [8], the effects of applied tensile stress on the growth of ellipsoidal ω-precipitates are examined for the same Ti–20Mo alloy aged at 300 °C. We have observed the stress-assisted growth of ω-precipitates, which depends on the sign of the misfit strain $\varepsilon_M$ of ω-precipitates along the loading direction, and furthermore found a change in growth kinetics from diffusion-controlled growth of ω-precipitates under no stress to interface-controlled growth of ω-precipitates in the case of $\varepsilon_M > 0$ under a tensile stress of 400 – 550 MPa, as will be discussed later. Prior to this work, direct evidence was not provided for interface-controlled growth of precipitates. The interface velocity for various massive reactions has been reported to obey an interface-controlled growth law [10].

## Experimental

Sheets of a Ti–20Mo alloy were provided by Daido Steel Co., Ltd. The alloy sheets were cold-rolled to a 50% reduction in thickness and then spark-cut into specimen strips. The cross-section and gage length of the specimens for tensile aging were 1 mm × 5 mm and 20 mm, respectively. All the specimens were solution-treated at 950 °C for 2 h under vacuum and quenched in water. The solution treatment also induced complete recrystallization of the

specimens. The average grain size after the solution treatment was approximately 60 μm. The solution-treated specimens were then aged at 300 °C for 3 h under no stress (free aging). Free aging at 300 °C for 3 h induced complete nucleation of the ω-precipitates [8]. The aged specimens were further aged at 300 °C for various times either under an applied tensile stress of 300, 400, 450, 500, and 550 MPa (stress aging) or under no stress, using a creep testing device. Specimens aged at 300 °C under no stress and under a tensile stress of 300 – 550 MPa are hereafter referred to as 0F and 300 – 550T, respectively. The maximum applied stress of 550 MPa is approximately four-fifths the yield strength of the solution-treated specimen at 300 °C.

To examine whether the creep deformation due to dislocation motion occurred during stress aging, measurements of length changes $\varepsilon_T$ upon aging were conducted by measuring, with a micrometer, the distance between two scribed marks, approximately 8 mm apart, for the specimen tensile-stress-aged (TSA) at 550 MPa and 300 °C for 1 h after being free-aged (FA) at 300 °C for 3 h, and the specimen FA at 300 °C for 1 h after being FA at 300 °C for 3 h. A length change measurement was also performed for the specimen compressive-stress-aged (CSA) at 550 MPa and 300 °C for 1 h after being FA at 300 °C. The specimen for compressive aging had a cross-section of 2 mm × 5 mm and a gage length of 7 mm, and two marks were scribed 5 mm apart. The length change is defined as $\varepsilon_T = (l–l_0)/l_0$, where $l_0$ and $l$ are the length between the two marks before and after aging, respectively. The measurement accuracy of length change was on the order of $10^{-5}$ in strain. The lattice parameters of the solution-treated and aged specimens were measured by X-ray analysis using an X-ray diffractometer equipped with a Cu target.

Thin 0.2-mm-thick foils for transmission electron microscopy (TEM) observations were prepared by grinding the aged specimens with SiC papers and by electropolishing using a solution of 60 vol% methanol, 35 vol% 2-butoxyethanol and 5 vol% perchloric acid at

–20 °C and 15 V in a twin-jet electropolisher. Microscopy was performed using a JEOL 2010FEF microscope operated at 200 kV.

## Results

### Age-hardening curves

Figure 1 shows the aging time *t* dependence of the Vickers hardness of the Ti–20Mo specimens FA and TSA (500MPa) at 300 °C after being FA at 300 °C for 3 h. The microhardness of the TSA specimen initially increased more rapidly than that of the FA specimen. The TSA and FA specimens exhibited the same maximum hardnesses at approximately 80 h ($2.88\times10^5$ s) and 1440 h ($5.184\times10^6$ s). As will be noted later, the initially higher hardness at each time for the TSA specimen is a consequence of the promotion of precipitate growth under tensile stress.

### Size and misfit strain of ω-variants

Figure 2a, b presents dark-field TEM images of ω-precipitates in a grain in the Ti–20Mo specimen aged at 300 °C for 9 h under a tensile stress of 500 MPa after being FA at 300 °C. Figure 2c shows the corresponding $[113]_\beta$ selected-area diffraction pattern (SADP). Since the $(113)_\beta$ plane in the grain was nearly parallel to the specimen surface, the loading direction (LD) of the specimen is shown in Fig. 2a, b. To determine the LD on the TEM images, the LD was marked on the thin foil, and then the foil was carefully set in a specimen holder. Reflections due to two ω-variants, I and II, among the four possible crystallographically-equivalent ω-variants were present in the $[113]_\beta$ SADP. The dark-field images in Fig. 2a, b were acquired using reflections due to variants I and II, respectively. The

variants I and II aligned with the β-Ti matrix according to the following orientation relationship: $[1\bar{1}1]_\beta$ // $[0001]_{\omega1}$; $(\bar{2}\bar{1}1)_\beta$ // $(10\bar{1}0)_{\omega1}$; $(011)_\beta$ // $(\bar{1}2\bar{1}0)_{\omega1}$ and $[\bar{1}11]_\beta$ // $[0001]_{\omega2}$; $(\bar{1}\bar{2}1)_\beta$ // $(01\bar{1}0)_{\omega2}$; $(101)_\beta$ //$(\bar{2}110)_{\omega2}$. The variants I and II had an ellipsoidal shape elongated along $[4\bar{7}1]_\beta$ and $[\bar{7}41]_\beta$ on $(113)_\beta$. Figure 2d is a dark-field image taken using a reflection due to the variant II in the specimen FA at 300 °C for 9 h after being FA at 300 °C. Notably, in Fig. 2a, b, d, the precipitate size for the variant I in the grain in the TSA specimen is larger than that for the variant II in the same grain, which is nearly identical to that for the FA specimen.

Dark-field images of ω-precipitates in the Ti–20Mo specimen FA and TSA (500 MPa) at 300 °C for various times after being FA at 300 °C were taken with an incident electron beam along the <011> direction. All four ω-variants had an ellipsoidal shape elongated along $<111>_\beta$ [9], with an aspect ratio of about 2.3, irrespective of the application of tensile stress and aging time. Here, the shape of ω-precipitates is assumed to be a spheroid described in *x*-*y*-*z* coordinates by $x^2/r^2+y^2/r^2+z^2/l^2 \leq 1$, where $l \fallingdotseq 2.3r$. The diameter *d* of a sphere having the same volume as the ellipsoidal precipitate was then calculated. For example, the average values of *r* and *l* were measured as 1.0 and 2.3 nm, respectively, after the specimen had been solutionized at 950 °C and then FA at 300 °C for 3 h. About 200 precipitates were used for measurements of *r* and *l*. Accordingly, the average diameter $d_0$ of the ω-precipitates was estimated as 2.7 nm.

In our previous study [8], we reported that the number density of a ω-variant in the Ti–20Mo specimen TSA at 300 °C is closely related to the misfit strain along the LD between the ω-variant and the matrix. We thus speculated that the difference in the size between the variants I and II in Fig. 1a, b is due to the difference in the misfit strain along the LD between them.

We often observed grains in which the $(113)_\beta$ plane was nearly parallel to the

surfaces of the TSA and FA specimens. The grains in which the $(113)_\beta$ plane was parallel to the specimen surfaces were used to estimate the misfit strains of the variants I and II along the LD on $(113)_\beta$. The angle $\phi$ between the LD and the elongated $[4\bar{7}1]_\beta$ or $[\bar{7}41]_\beta$ direction of variant I or II on $(113)_\beta$ in the grain (see Fig. 2a, b) was first measured, the LD, i.e., $[h\ k\ l]_\beta$ and $[p\ q\ r\ s]_\omega$, was then calculated under the condition of $h^2 \leq 225$, $k^2 \leq 225$, $l^2 \leq 225$, $p^2 \leq 225$, $q^2 \leq 225$, $r^2 \leq 225$ and $s^2 \leq 225$, and the spacings $D_\beta$ and $D_\omega$ of the planes perpendicular to $[h\ k\ l]_\beta$ and $[p\ q\ r\ s]_\omega$ were estimated. The misfit strain $\varepsilon_M$ of the variant I or II along the LD on $(113)_\beta$ was calculated using:

$$\varepsilon_M = (D_\omega - D_\beta) / D_\beta \tag{1}$$

In the case of the variants I and II along the LD in Fig. 2a, b, the estimated values of $\varepsilon_M$ were 0.12 and −0.01, respectively.

The actual elongated directions of the variants I and II in Fig. 2a, b were along $[1\bar{1}1]_\beta$ and $[\bar{1}11]_\beta$, respectively. To obtain values of $d$ for the variants I and II, sizes of ω-precipitates of the variants along $[4\bar{7}1]_\beta$ and $[\bar{7}41]_\beta$ on $(113)_\beta$ were measured and then were converted into values of $l$ along $[1\bar{1}1]_\beta$ on $(011)_\beta$ and $[\bar{1}11]_\beta$ on $(101)_\beta$. The average values of $r$ and $l$ for the variants I and II in Fig. 2a, b were estimated as 3.9 and 9.6 nm, and 2.1 and 5.0 nm, respectively. About 100 precipitates were used for measurements of $r$ and $l$ for each variant. Accordingly, the average values of $d$ for the variants I and II were 10 and 5.7 nm, respectively. Similarly, we obtained average values of $d$ for the variants I and II in the other grains in which the $(113)_\beta$ plane was parallel to the surfaces of the TSA specimens.

Figure 3 presents the growth size $d - d_0$ of variants I and II, plotted as a function of the misfit strain $\varepsilon_M$ of precipitates along the LD for the specimens TSA (500 MPa) and FA at 300 °C for 9 h. The average value of $d - d_0$ for the FA specimen was 2.8 nm, as indicated by the solid line in Fig. 3. Several large misfit strains, such as 0.25 and 0.29, are evident in Fig. 3.

However, the actual misfit strains may be small, because a large misfit strain can be relieved by an array of misfit dislocations at the interface between different phases [7, 11]. Figure 3 demonstrates that the values of $d - d_0$ for the TSA specimen are larger than that for the FA specimen when $\varepsilon_M > 0$, whereas they are nearly identical to that for the FA specimen when $\varepsilon_M < 0$. The growth of the ω-variants was observed to be promoted in the specimens aged at 300 °C under a tensile stress of 300 – 550 MPa in the case $\varepsilon_M > 0$; however, the tensile stress did not significantly affect the growth of the variants when $\varepsilon_M < 0$. Hereafter, ω-variants I and II in the case $\varepsilon_M > 0$ in specimens aged at 300 °C under a tensile stress of 300, 400, 450, 500, and 550 MPa are referred to as 300TL, 400TL, 450TL, 500TL and 550TL respectively, and variants in the case $\varepsilon_M < 0$ in specimens aged at 300 °C under a tensile stress of 300 – 550 MPa are referred to as 300 – 550TS.

Growth kinetics

Figure 4a displays the growth size $d - d_0$ plotted against aging time $t$ on logarithmic scales for ω-variants 500TL and 500TS and for ω-variants in specimens 0F and 500T. In the initial stage of aging, a linear relationship was observed between log $(d - d_0)$ and log $t$ for all of the specimens, which indicates that $(d - d_0)^n$ is nearly proportional to $t$. In the case of 0F and 500TS, $n$ was approximately 2; however, in the case of 500TL, $n$ was approximately 1. For 500T, $n$ was between 1 and 2.

Figure 4b, c presents the lattice parameter $a_\beta$ of the β-Ti matrix and the lattice parameters $a_\omega$ and $c_\omega$ of the ω-precipitates with a hexagonal structure, measured by X-ray analysis, as a function of $t$ for specimens 500T and 0F. The lattice parameter of the β-Ti matrix decreases with increasing $t$ for 500T and 0F; however, the lattice parameters of the ω-precipitates increase. Mo atoms diffuse from the ω/β interface toward the β-Ti matrix as

the ω-precipitates grow [12]. Because Mo atoms are smaller than Ti atoms, the increase in the concentration of Mo atoms within the β-Ti matrix and the decrease in the Mo concentration within the ω-precipitates resulted in a decrease of the β-Ti lattice parameter and increases of the lattice parameters of the ω-phase, respectively. In addition, the lattice parameter of the β-Ti matrix in 500T decreases more rapidly than that in 0F and then saturates to the value of 0.3231 nm over 48 h ($1.728 \times 10^5$ s). This value is close to the lattice parameter, 0.3229 nm, of a β-Ti solid solution containing 39wt%Mo that is the equilibrium solubility of Mo in β-Ti at 300 °C in the Ti-Mo binary phase diagram [12]. The value of 0.3229 nm was estimated using the experimental data reported for the dependence of the lattice parameter on the Mo concentration ($\Delta a_\beta$ = –0.0002 nm/at%) in the literature [13]. Moreover, Figure 4c shows that the lattice parameters of the ω-precipitates in 500T increase more rapidly than those in 0F and then saturate to the values of $a_\omega$=0.2836 nm and $c_\omega$=0.4679 nm over about 48 h. Although experimental data regarding the dependence of the lattice parameters of ω-precipitates on the Mo concentration have not yet been reported, these values are believed to be close to the lattice parameters of an ω solid solution containing 10wt%Mo that is the equilibrium solubility of Mo in ω-precipitates at 300 °C in the Ti-Mo binary phase diagram [12].

Figure 4d presents the number density $N$ of ω-variants as a function of $t$ for 500T and 0F. The number density of ω-precipitates is defined as the volume fraction $f$ of precipitates divided by the average volume of a single precipitate ($N=3f/4\pi(d/2)^3$). Approximately 600 precipitates were used for estimates of $d$ at each aging time. The volume fraction was determined by applying the lattice parameters of the β-Ti matrix in 500T and 0F in Fig. 4b to the experimental data reported for the dependence of the lattice parameter on the Mo concentration [13]. The lattice parameters of the ω-precipitates as a function of $t$ for 500T and 0F in Fig. 4c were also used in this calculation. In addition, the concentration of Mo in the ω-precipitates was assumed to be 10wt%, as mentioned above.

Figure 4d demonstrates that, in the case of specimen 500T, the number density of ω-precipitates is constant from 2 to 10 h and then rapidly decreases, whereas, in the case of 0F, it remains constant from 2 to 165 h ($5.94 \times 10^5$ s). Notably, a linear relationship is seen between log $(d-d_0)$ and log $t$ from 2 to 10 h for 500TL and from 2 to 165 h for 0F in Fig. 4a. Therefore, in the growth stage of ω-precipitates after nucleation, the values of $n$ for 0F and 500TL are approximately 2 and 1, respectively.

Fratzl et al. [14], who used small-angle X-ray scattering to study the growth of ω-precipitates in a Ti–20at%Mo (33.4wt%Mo) alloy aged at temperatures below 500 °C, observed that the precipitate size $r$ increases, in a first step, as $r \propto t^{1/3}$ with increasing aging time $t$, but then stabilizes at a constant value of $r$=7.5 nm. The former result is in disagreement with our result that, during the growth stage of ω-precipitates in specimen 0F, the size $d$ increases as $d \propto t^{1/2}$ with increasing $t$.

Figure 5 shows the growth size $d-d_0$ as a function of $t$ on logarithmic scales for 300 – 550TL. A linear relationship exists between log $(d-d_0)$ and log $t$ for 300 – 550TL. The values of $n$ are obtained from the slopes of the straight lines obtained by the least-squares method. The calculated values are listed in Table 1. For 400–550TL, $n \doteqdot 1$. For 300 – 550TS, the values of $n$ were approximately 2. Figure 6 shows a replot of the growth size $d-d_0$ against $t$ for 400 – 550TL. The growth rates were obtained from the slopes of the straight lines. The growth rate $v$ plotted against tensile stress $\sigma$ is shown in Fig. 7. The growth rate increases linearly with increasing tensile stress.

Table 2 lists the length change $\varepsilon_T$ along the LD for specimens FA, TSA and CSA (550 MPa) at 300 °C for 1 h after the specimens were FA at 300 °C for 3 h. The FA specimen exhibits no change in length within the experimental error. However, length change along the LD for the TSA and CSA specimens exhibits a slight decrease. These results indicate that the creep strain due to dislocation motion does not contribute to the length change. The specimen

length-change $\varepsilon_T$ along any direction can be represented as functions of the average misfit strain along a direction caused by the misfit strains of precipitates along the direction, the volume fraction $f$ of the precipitates, and the dimensional change due to the change in solute atoms in the solid solution [11, 15].

Temperature dependence of precipitate size

Figure 8 shows the growth size $d - d_0$ plotted against aging temperature $T$ for specimens isochronally FA for 2 and 12 h. In Fig. 9, 2- and 4-h isochronal aging as a function of $T$ are presented for variants I and II in the case $\varepsilon_M > 0$ in the specimens aged under a tensile stress of 500 MPa. For a specimen TSA at the maximum temperature of 623 K (350 °C) in Fig. 9, the value of $n$ was observed to be approximately 1.0. In Figs. 8 and 9, at a given aging temperature, the value of $d - d_0$ is larger as the aging time is longer.

**Discussion**

As mentioned in the preceding section, exponent $n \fallingdotseq 2$ for 0F and 300–550TS, but $n \fallingdotseq 1$ for 400–550TL. An $n$-value of 2 indicates that the growth kinetics of the ω-variants follows a diffusion-controlled parabolic growth law, whereas a value of 1 indicates that the growth of the ω-variants obeys an interface-controlled growth law [16]. Consequently, while the growth of ω-precipitates under no stress or in the case $\varepsilon_M < 0$ under tensile stress is governed by the diffusion of Mo atoms from the β/ω interface toward the β-Ti matrix [10, 16], precipitate growth is instead interface-controlled in the case $\varepsilon_M > 0$ under tensile stress.

In diffusion-controlled growth, the size $s$ of spherical precipitates or the thickness of plate-shaped precipitates theoretically follows a parabolic growth law:

$$s = \alpha\sqrt{t}, \tag{2}$$

where $\alpha$ is the parabolic rate constant and $t$ is the growth time. The linearized concentration gradient model of Zener [17] gives the parabolic rate constant as:

$$\alpha = (X_\beta^{\beta\omega} - X_\beta)\sqrt{D} / \sqrt{(X_\beta^{\beta\omega} - X_\omega^{\omega\beta})(X_\beta - X_\omega^{\omega\beta})}, \tag{3}$$

where $D$ is the volume diffusivity of solute in the β-matrix, $X_\beta$ is the mole fraction of solute in the bulk alloy, $X_\beta^{\beta\omega}$ is the mole fraction of solute in β for (ω+β) equilibrium, and $X_\beta^{\omega\beta}$ is the mole fraction of solute in ω for (ω+β) equilibrium. The thickening of plate-shaped precipitates and grain-boundary allotriomorphs in several alloy systems, for example, the thickening of Cr-rich precipitates with a lath morphology in a Ni-Cr alloy [18] and plate-shaped γ-precipitates in a Cu–Ni–Be alloy [19], have been reported to occur with parabolic growth kinetics [10]. In contrast, in the case of interface-controlled growth of a precipitate, the interface velocity $v_I$ may be written as [16]:

$$v_I = \delta\nu(\Delta G_m / RT)\exp(-\Delta G_d / RT), \tag{4}$$

where $\delta$ is the interface width, $\nu$ is the vibrational attempt frequency, $\Delta G_m$ is the difference in free energies per mol between the β- and ω-phases, $\Delta G_d$ is the activation energy for interface transport, and $R$ and $T$ have their usual meanings. Although the interface velocity for various massive reactions has been observed to obey the interface-controlled growth equation [10], direct evidence has not yet been provided for the interface-controlled growth of precipitates. Massive transformation is one in which the product phase has the same composition as the matrix and the migration mechanism of the interface boundaries is diffusion across these boundaries.

The origin of the misfit strain dependence of the growth of ω-variants (Figs. 3 and

4a) and the relationship between the growth rate of ω-variants and tensile stress (Fig. 7) can be understood to arise through the interaction energy between an external stress $\sigma_{ij}$ and a misfit strain $\varepsilon_{ij}$ (stress-free transformation strain). The interaction energy per unit volume of a precipitate is expressed as [20]:

$$F_I = -\sigma_{ij}\varepsilon_{ij}. \quad (5)$$

That is, the interaction energy is the work done by the external stress during the ω-precipitate growth. When $\varepsilon_{ij} > 0$, the amount of work done by an applied tensile stress $\sigma_{ij}$ (> 0) is $|F_I| = |-\sigma_{ij}\varepsilon_{ij}|$. We think that the sum of the driving force per mol $\Delta G_m$ and the work done by an external stress $|F_I|V_m$ is the total driving force under the external stress. Here $V_m$ is the molar volume of the precipitate. Thus, the interface velocity under an external stress $\sigma_{ij}$ may be expressed as:

$$v_I = \delta\nu[(\Delta G_m + |F_I|V_m)/RT]\exp(-\Delta G_d/RT). \quad (6)$$

As mentioned in the preceding section, the concentration of Mo atoms within the β-Ti matrix or within the ω-precipitates initially increases or decreases with increasing aging time. Changes in the Mo concentration within the matrix and the precipitates may result in a decrease in $\Delta G_m$. In this work, the amount of change in $\Delta G_m$ is assumed to be small in the growth stage of the ω-precipitates.

Equations 5 and 6 predict that applied tensile stress promotes the growth of the ω-variants when $\varepsilon_M > 0$, but does not affect it when $\varepsilon_M < 0$. This prediction is in agreement with the results shown in Figs. 3 and 4(a). On the basis of Eqs. 5 and 6, the growth rate of ω-variants is also expected to be proportional to the tensile stress, as is the case in Fig. 7.

As evident in Eqs. 2 and 3, in a diffusion-controlled reaction, a linear dimension of the growing product region is proportional to the square root of the growth time, whereas, in

an interface-controlled reaction, it is linearly proportional to the time. Thus, an interface-controlled boundary of a very small product region may become diffusion-controlled as the region grows larger [16]. Actually, the thickening and lengthening of plate-shaped precipitates of large sizes in several alloy systems have been observed to be diffusion-controlled [10]. In this study also, the growth of the ω-precipitates with sizes larger than 2.7 nm in average diameter under no stress is governed by the diffusion of Mo atoms from the β/ω interface toward the β-Ti matrix. However, under a tensile stress of $400-550$ MPa, the growth of precipitates smaller than about 13 nm is interface-controlled when $\varepsilon_M > 0$ (Figs. 4a and 5). The velocity of the interface-controlled growth increases with increasing tensile stress (Figs. 6 and 7). Therefore, the parabolic rate constant α (Eqs. 2 and 3) expected under tensile stress would be much larger than that under no stress.

Equations 2 and 3 indicate that the activation energy $\Delta G_v$ for the volume diffusivity of Mo in the β matrix can be obtained by the cross-cut method, using the results of two isochronal aging treatments for precipitates of the same size; i.e., $\Delta G_v$ can be determined using:

$$t_1 \exp(-\Delta G_v / RT_1) = t_2 \exp(-\Delta G_v / RT_2), \quad (7)$$

where $t_1$ and $t_2$ are the times required to achieve the same size of precipitates at aging temperatures $T_1$ and $T_2$, respectively. Using the data shown in Fig. 8, we determined the activation energy to be approximately 190 kJ/mol. This value is similar to that of 180 kJ/mol previously reported for the volume diffusion of Mo in β-Ti [21]. Similarly, the activation energy $\Delta G_d$ for interface transport in Eq. 4 can be calculated using the following equation:

$$(t_1 / T_1) \exp(-\Delta G_d / RT_1) = (t_2 / T_2) \exp(-\Delta G_d / RT_2) \quad (8)$$

The activation energy determined using Fig. 9 was approximately 130 kJ/mol. This value is

appreciably smaller than the value of $\Delta G_v$ (≒190 kJ/mol).

The interface velocity for various massive reactions has been observed to obey the interface-controlled growth equation [10]. For various massive reactions, estimated values of $\Delta G_d$ were similar to those expected for grain-boundary diffusion. In this study, the value of $\Delta G_d$ (≒130 kJ/mol) is approximately 70% of the value of $\Delta G_v$, and is smaller than the activation energy of 153 kJ/mol for self-diffusion of β-Ti [22]. Therefore, the value of 130 kJ/mol is reasonably identified as the activation energy for grain-boundary diffusion.

Finally, values of $\Delta G_m$ and $|F_I|V_m$ in Eq. 4 are compared. The value of $\Delta G_m$ at 300 °C for the Ti–20Mo alloy is calculated using the literature [23] to be approximately 240 J/mol. However, a portion of $\Delta G_m$ ≒ 240 J/mol may be dissipated by diffusion processes [24]. When calculated using $\sigma$=400 – 550 MPa, $\varepsilon_M$=0.05 and $V_m$=1.03 x $10^{-5}$ $m^3$/mol, the value of $|F_I|V_m$ is estimated as 220 – 280 J/mol. The values of $|F_I|V_m$ are comparable to the value of $\Delta G_m$. Because the average misfit strain of the ω-precipitate, calculated from the lattice parameters of the β-Ti matrix and the ω-precipitate, is 0.010 [8], the average of the positive misfit strains (Fig. 3) must be greater than 0.010. In addition, large misfit strains between different phases are reported to become smaller than approximately 0.1 after relief by an array of misfit dislocations at the interface [7, 11]. Thus, the value of $\varepsilon_M$ = 0.05 is assumed in this work.

## Conclusions

Our investigation of the growth of ellipsoidal ω-phase precipitates in a Ti-20wt%Mo alloy aged at 300°C under an applied tensile stress of 300–550MPa or under no stress yielded the following conclusions:

1. The application of tensile stress promotes the growth of ω-precipitates when the misfit strain $\varepsilon_M$ of the precipitates along the loading direction is greater than 0; however it does

not significantly affect the growth of precipitates when $\varepsilon_M < 0$.

2. The ω-precipitates in the alloy aged under no stress grow with parabolic growth kinetics. Tensile stress does not affect the growth kinetics when $\varepsilon_M < 0$, whereas, in the case $\varepsilon_M > 0$ under a tensile stress of 400 – 550 MPa, precipitate size increases linearly with increasing aging time. This observation indicates that although the growth of ω precipitates under no stress or in the case $\varepsilon_M < 0$ under tensile stress is controlled by the diffusion of Mo from the ω/β interface toward the β-Ti matrix, precipitate growth is instead interface-controlled in the case $\varepsilon_M > 0$ under a tensile stress of 400 – 550 MPa.
3. The growth velocity of the precipitates in the case $\varepsilon_M > 0$ is proportional to the tensile stress.
4. The misfit strain dependence of the growth of precipitates and the stress dependence of the growth rate of precipitates are explained on the basis of the interaction energy due to the presence of misfit strains between the applied stress and the ω-precipitates.
5. The activation energies for the interface-controlled and diffusion-controlled reactions are estimated to be approximately 130 and 190 kJ/mol, respectively. The latter value is consistent with the activation energy for the bulk diffusion of Mo in β-Ti [21].

## References


1. Hosford WF, Agrawal SP (1975) Effect of stress during aging on the precipitation of $\theta'$ in Al-4 Wt pct Cu, Metall Mater Trans A 6: 487-491
2. Eto T, Sato A, Mori T (1978) Stress-oriented precipitation of G. P. Zones and $\theta'$ in an Al-Cu alloy, Acta Metall 26: 499-508
3. Skrotzki B, Shiflet G, Starke Jr EA (1996) On the effect of stress on nucleation and growth of precipitates in an Al-Cu-Mg-Ag alloy, Metall Mater Trans A 27: 3431-3444
4. Zhu AW, Starke Jr EA (2001) Stress aging of Al–xCu alloys: experiments, Acta Metall 49: 2285-2295
5. Chen JF, Zou LC, Chen YL, Li Q (2015) Effect of stress on precipitation behaviour of 7xxx alloy during age forming process. Mater. Sci. Technol. doi: 10.1179/1743284715Y.0000000100
6. Monzen R, Watanabe C, Seo T, Sakai T (2005) Effect of applied stress on precipitation of Guinier–Preston zones in a Cu–0.9 wt% Be single crystal, Phil Mag Lett 85: 603-612
7. Monzen R, Okawara S, Watanabe C (2012) Stress-assisted nucleation and growth of γ″and γ′ precipitates in a Cu–1.2 wt%Be–0.1 wt%Co alloy aged at 320°C, Phil Mag 92: 1826-1843
8. Monzen R, Kawai R, Watanabe C (2015) Effect of external stress on nucleation of ellipsoidal ω precipitates in a Ti-20wt%Mo alloy, J Mater Sci 50: 1876-1882
9. Fontaine DD, Paton NE, Williams JC (1971) The omega phase transformation titanium alloys as an example of displacement controlled reactions, Acta Metall 19: 1153-1162
10. Aaronson HI, Enomoto M, Lee JK(2010) Mechanisms of Diffusional Phase Transformations in Metals and Alloys, CRC Press, New York

11. Watanabe C, Sakai T, Monzen R (2008) Misfit strains of precipitated phases and dimensional changes in Cu–Be alloys, Phil Mag 88: 1401-1410
12. Hickman BS (1969) Omega phase precipitation in alloys of titanium with transition Metals, Trans Metall Soc AIME 245: 1329-1336
13. Kun S, Xuezhong Y, Erdong W, Dongfeng C, Cheng G (2006) Neutron diffraction study of the deuterides of Ti-Mo alloys, Physica B 385-386: 141-143
14. Fratzl P, Langmayr F, Vogl G, Miekeley W (1991) The growth of ω-phase inclusions in Ti-20at%Mo and the competition between elastic and surface energies, Acta Metall 39: 753-761
15. Monzen R, Hasegawa T, Watanabe C (2010) Effect of external stress on discontinuous precipitation in a Cu-2.1wt%Be alloy, Phil Mag 90: 1347-1358
16. Christian JW (2002) The theory of in Metals and Alloys, 3rd ed., 1, Pergamon Press, Oxford
17. Zener C (1949) Theory of growth of sperical precipitates from solid solution, J Appl Phys 20: 950-952
18. Chen G, Spanos G, Matsumura RA, Reynolds Jr WT (2005) Effect of ledgs density on the morphology and growth kinetics of precipitates in a Ni-Cr alloy, Acta Mater 53: 895-906
19. Watanabe C, Monzen R (2011) Precipitation process in a Cu-Ni-Be alloy, Solid State Phenom 172-174:432-436
20. Eshelby JD (1957) The determination of the elastic field of an ellipsoidal inclusion, and related problems, Proc R Soc A 241: 376-396
21. Gibbs GB, Graham D, Tomlin DH (1963) Diffusion in titanium and titanium-niobium alloys, Phil Mag 8: 1269-1282
22. Walsöe NE, Libanati GM (1968) Autodifusion de Titanio beta y Hafnio, Acta Metall 16: 1297-1305

23. Leibovitch Ch, Rabinkin A (1980) Metastable diffusionless equilibria in Ti-Mo and Ti-V systems under high pressure conditions, Calphad 4: 13-26

24. Hillert M (1974) Diffusion and interface control of reactions in alloy, Met Trans A 6: 5-19

**Figure and Table Captions**

**Fig. 1** Age-hardening curves of Ti–Mo specimens free-aged (FA) and tensile-stress-aged (TSA) (500 MPa) at 300 °C after being FA at 300 °C for 3 h. Representative error bars are shown

**Fig. 2 a, b** Dark-field TEM images of ω-variants I and II in a Ti–Mo specimen tensile-stress-aged (TSA) (500 MPa) at 300 °C for 9 h after being free-aged (FA) at 300 °C for 3 h. *LD* loading direction. **c** $[113]_\beta$ selected-area diffraction pattern corresponding to (a and b). **d** Dark-field image of ω-variant II in a Ti-Mo specimen FA at 300 °C for 9 h after being FA at 300 °C for 3 h

**Fig. 3** Growth size $d - d_0$ for ω-variants I and II in Ti-Mo specimens tensile-stress-aged (TSA) (500 MPa) and free-aged (FA) at 300 °C for 9 h after being FA at 300 °C for 3 h; the growth size is plotted as a function of the misfit strain $\varepsilon_M$ of ω-precipitates along the loading direction

**Fig. 4** Aging time $t$ dependence of **a** the growth size $d - d_0$ for 500TL and 500TS and ω-variants in 0F and 500T, **b** the lattice parameter $a_\beta$ of the β-Ti matrix in 0F and 500T, **c** the lattice parameters $a_\omega$ and $c_\omega$ of the ω-precipitates in 0F and 500T, and **d** the number density $N$ of ω-variants in 0F and 500T. Representative error bars are shown

**Fig. 5** Growth size $d - d_0$ plotted against aging time $t$ on logarithmic scales for 300, 400, 450, 500, and 550TL. Representative error bars are shown

**Fig. 6** Growth size $d - d_0$ against aging time $t$ for 400, 450, 500, and 550TL. Representative error bars are shown

**Fig. 7** Tensile stress $\sigma$ dependence of the growth rate $v$ for 400, 450, 500, and 550TL. A representative error bar is shown

**Fig. 8** Temperature $T$ dependence of the growth size $d - d_0$ for specimens isochronally free-aged for 2 and 12 h. Representative error bars are shown

**Fig. 9** Temperature $T$ dependence of the growth size $d - d_0$ for ω-variants I and II in the case $\varepsilon_M > 0$ in specimens isochronally aged for 2 and 4 h under a tensile stress of 500 MPa. Representative error bars are shown

**Table 1** Calculated $n$ values for 300, 400, 450, 500, and 550TL

**Table 2** Length change $\varepsilon_T$ along the loading direction for specimens free-aged (FA), tensile-stress-aged (TSA) and compressive-stress-aged (CSA) (550 MPa) at 300 °C for 1 h after being FA at 300 °C for 3 h

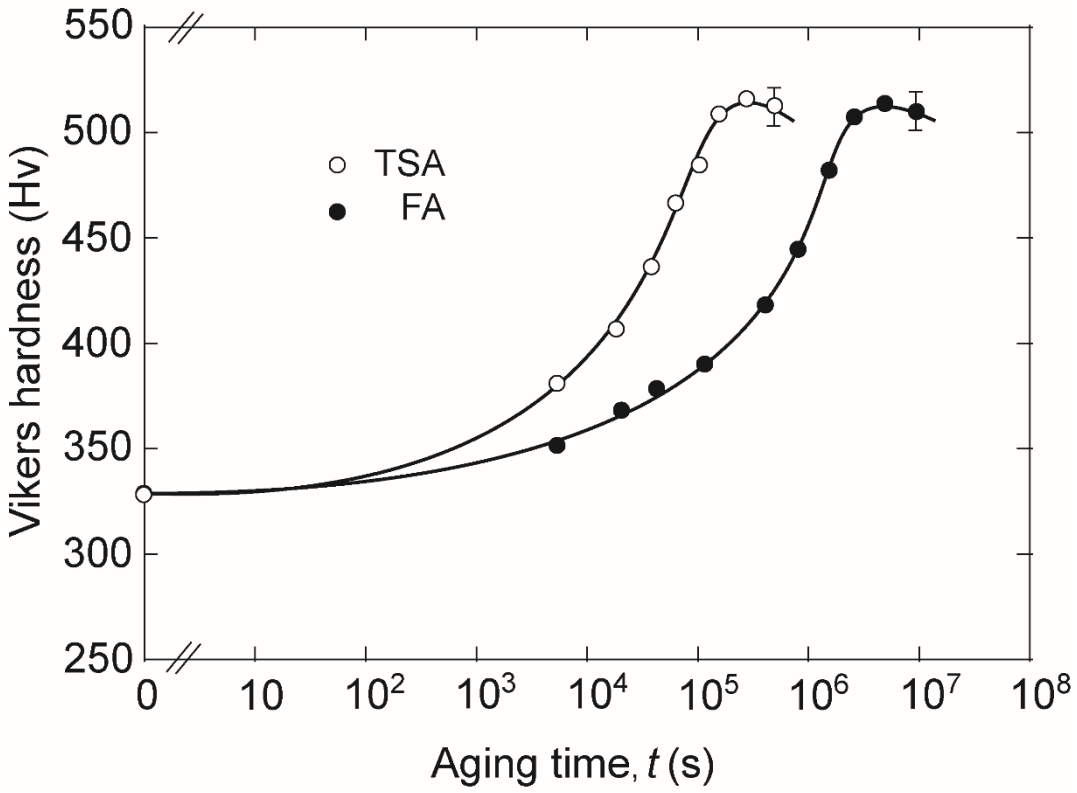
550
500
450
400
350
300
250
Vikers hardness (Hv)
TSA
FA
0
10
10^2
10^3
10^4
10^5
10^6
10^7
10^8
Aging time, t (s)

Fig. 1

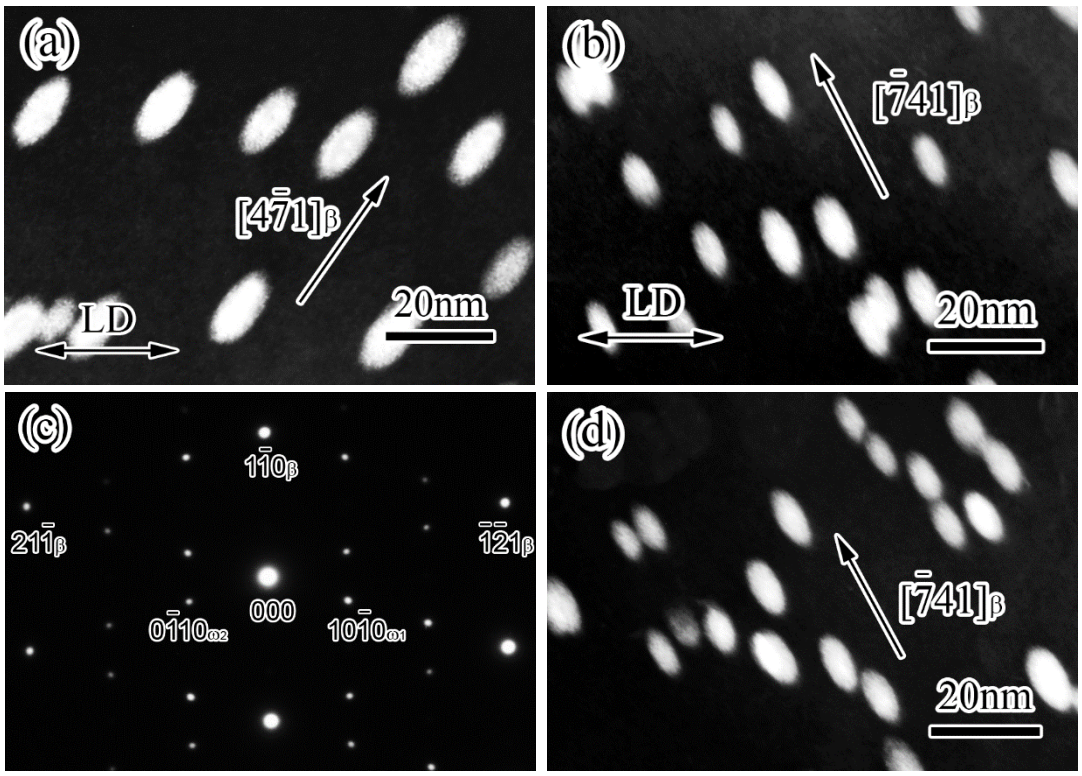
(a)
$[4\bar{7}\bar{1}]_\beta$
LD
20nm
(b)
$[\bar{7}41]_\beta$
LD
20nm
(c)
$1\bar{1}0_\beta$
$21\bar{1}_\beta$
$\bar{1}\bar{2}1_\beta$
000
$0\bar{1}10_{\omega 2}$
$10\bar{1}0_{\omega 1}$
(d)
$[\bar{7}41]_\beta$
20nm

Fig. 2

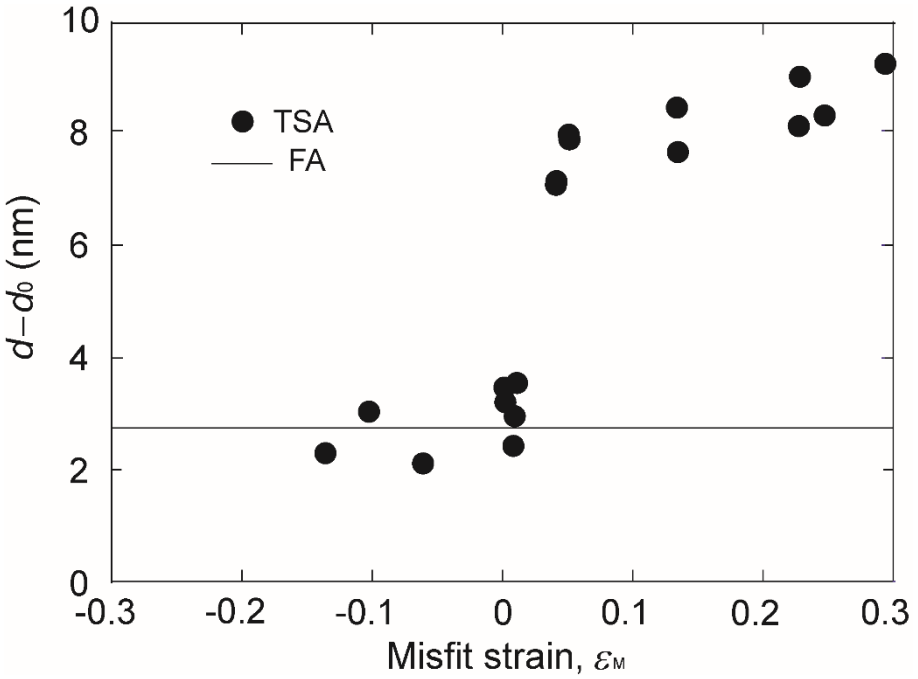


Fig. 3

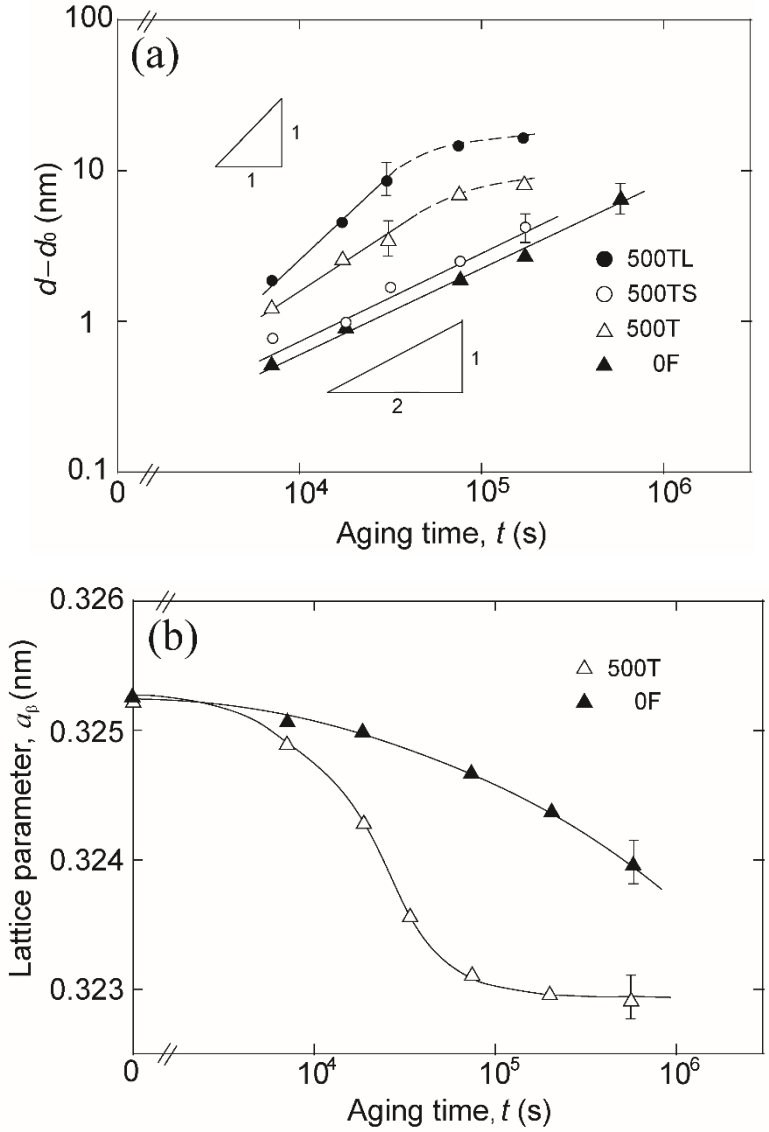
(a)
100
10
1
0.1
0
$10^4$
$10^5$
$10^6$
$d-d_0$ (nm)
Aging time, $t$ (s)
1
1
1
2
500TL
500TS
500T
0F
(b)
0.326
0.325
0.324
0.323
Lattice parameter, $a_\beta$ (nm)
500T
0F

Fig. 4

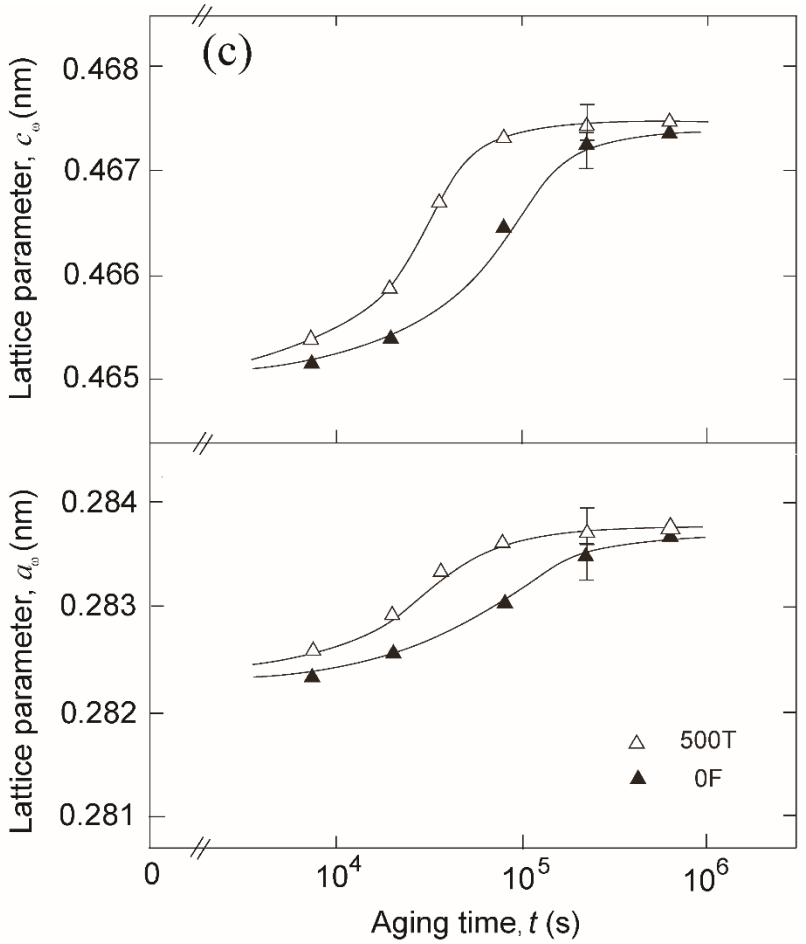
(c)
Lattice parameter, $c_\omega$ (nm)
0.468
0.467
0.466
0.465
Lattice parameter, $a_\omega$ (nm)
0.284
0.283
0.282
0.281
500T
0F
0
$10^4$
$10^5$
$10^6$
Aging time, $t$ (s)

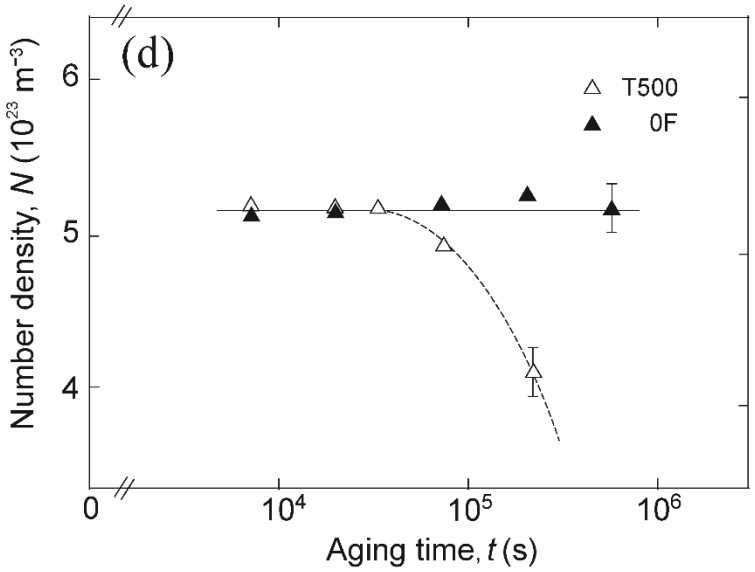
(d)
Number density, $N$ ($10^{23}$ m$^{-3}$)
6
5
4
T500
0F
0
$10^4$
$10^5$
$10^6$
Aging time, $t$ (s)

Fig. 4

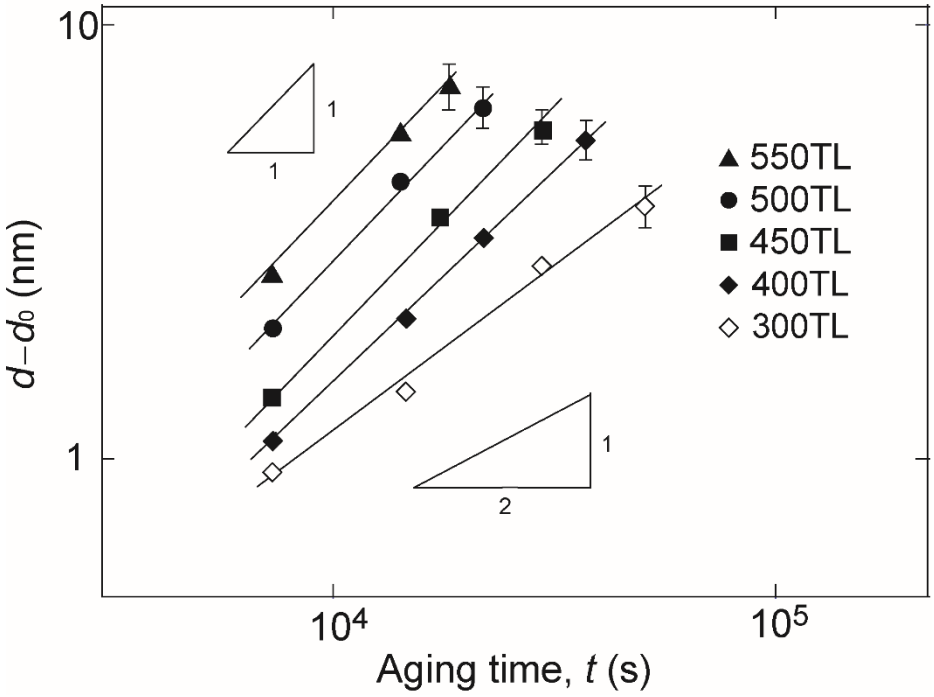
10
1
$d-d_0$ (nm)
1
1
1
2
550TL
500TL
450TL
400TL
300TL
$10^4$
$10^5$
Aging time, $t$ (s)

Fig. 5

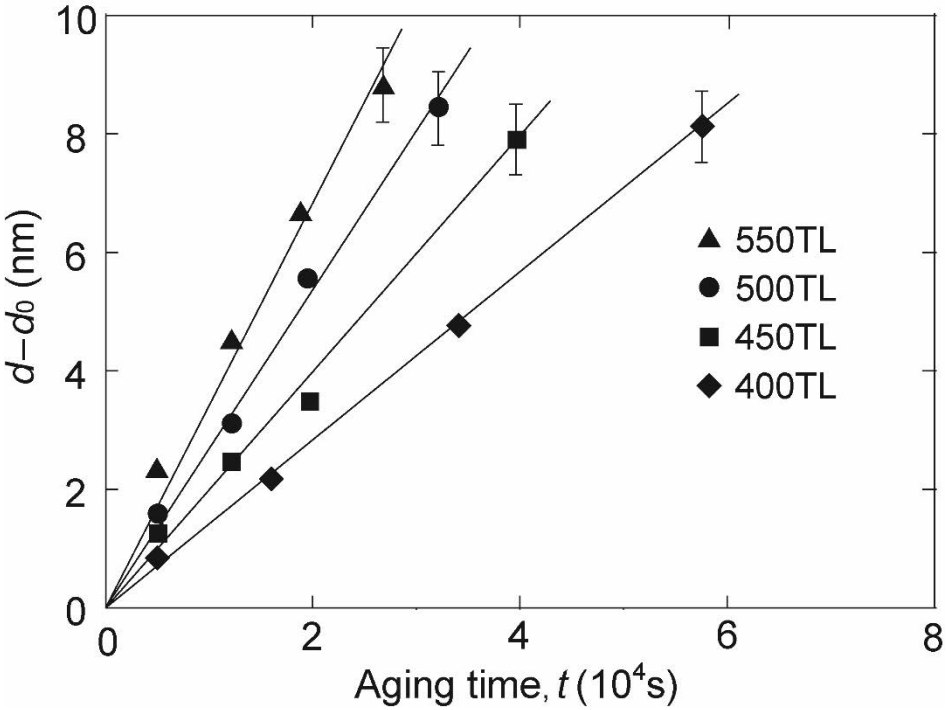
10
8
6
4
2
0
0
2
4
6
8
d−d0 (nm)
Aging time, t (10^4s)
550TL
500TL
450TL
400TL

Fig. 6

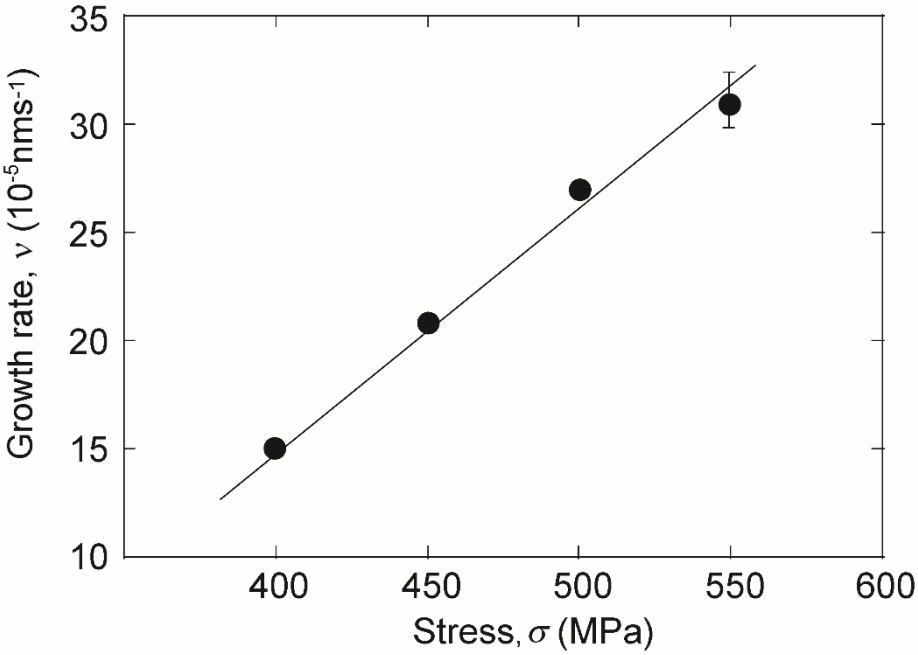
35
30
25
20
15
10
400
450
500
550
600
Growth rate, v (10-5nms-1)
Stress, σ (MPa)

Fig. 7

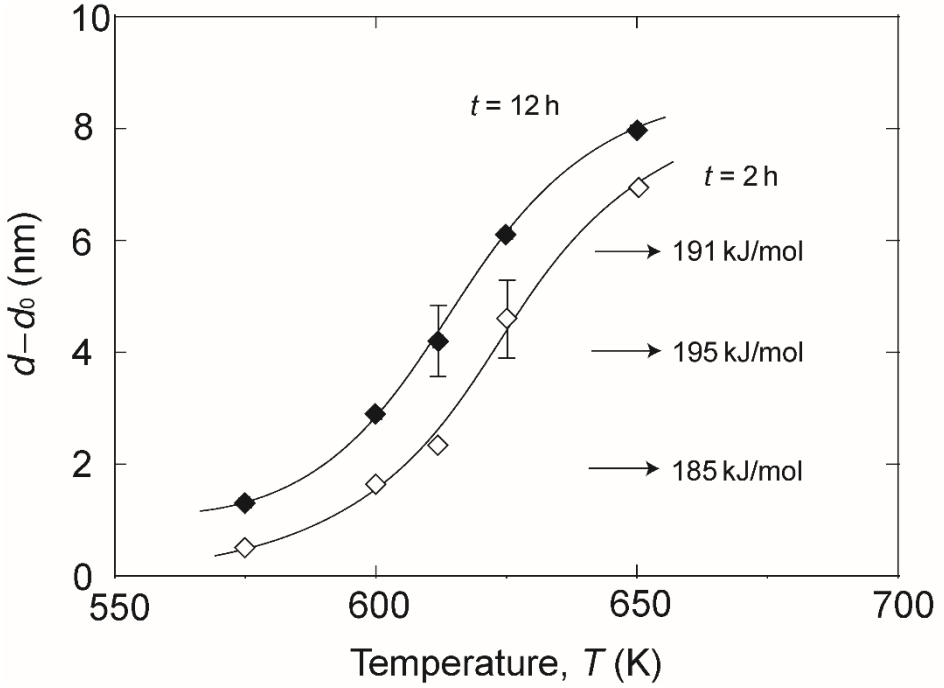
10
8
6
4
2
0
550
600
650
700
$d-d_0$ (nm)
Temperature, $T$ (K)
$t$ = 12 h
$t$ = 2 h
191 kJ/mol
195 kJ/mol
185 kJ/mol

Fig. 8

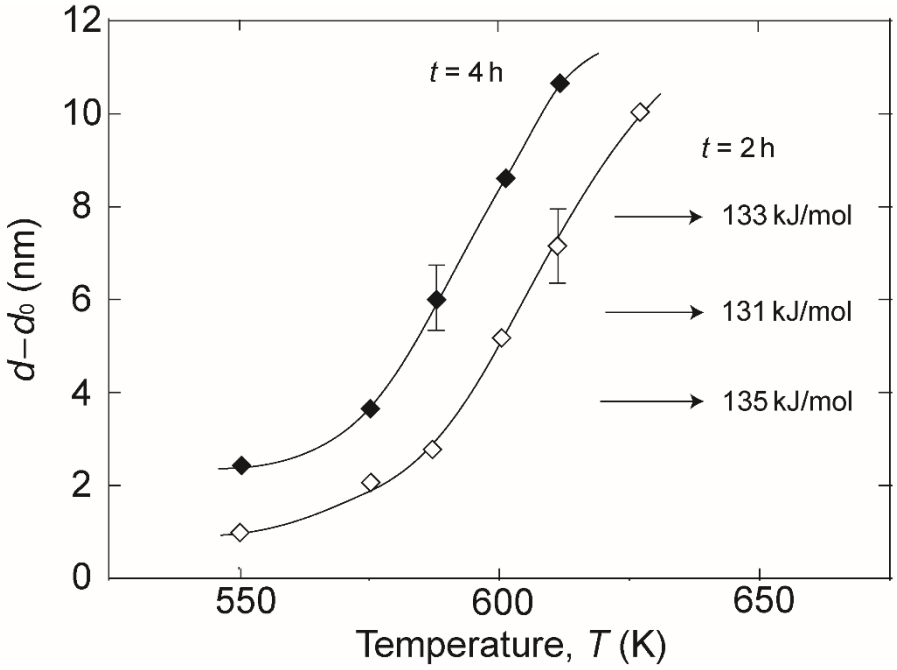
12
10
8
6
4
2
0
d–d0 (nm)
550
600
650
Temperature, T (K)
t = 4 h
t = 2 h
133 kJ/mol
131 kJ/mol
135 kJ/mol

Fig. 9

Table 1

| Variant | 300TL | 400TL | 450TL | 500TL | 550TL |
|---|---|---|---|---|---|
| $n$ | 1.5±0.1 | 1.1±0.1 | 1.0±0.2 | 1.1±0.2 | 1.0±0.2 |

Table 2

| Specimen | FA | TSA | CSA |
|---|---|---|---|
| $\varepsilon_T\,(10^{-3})$ | 0 ± 0.2 | - 1 ± 0.2 | - 0.5 ± 0.2 |